Thermo-physical properties of bulk Gd_2O_3 for fuel performance analysis of a lumped burnable absorber fuel design

Qusai Mistarihi, Faris B. Sweidan, and Ho Jin Ryu*
[b]*Korea Advanced Institute of Science and Technology, Nuclear & Quantum Engineering Dept. 291 Daehakro, Yuseong, 34141, Republic of Korea*
[*]*Corresponding author: hojinryu@kaist.ac.kr*

1. Introduction

Among the changes that have been made to increase the fuel cycle length, the loading of fissile materials has been increased. This presents an excess amount of reactivity that needs to be compensated for by the addition of neutron absorbing materials to avoid super-criticality. This can be achieved using control rods (CRs), by the addition of soluble boron to the reactor coolant as a chemical shim, and by the addition of burnable absorbers (BAs) [1]. The CRs insertion produces a non-uniform axial power distribution. On the other hand, the concentration of soluble boron in the reactor coolant is limited because of the positive moderator temperature coefficient (MTC) resulting from the reduction of the quantity of boron in the reactor coolant in response to the thermal expansion of water [2]. BAs have been developed to compensate for the CRs and chemical shim limitations in controlling the excess reactivity to allow for a further increase in the fuel cycle length [2]. Gadolinium sesquioxides (Gd_2O_3) is widely used as a burnable absorber (BA) material in light water reactors (LWRs) due to its high thermal neutron absorption cross-section. In comparison with other BA materials, Gd_2O_3 offers a reduced water displacement and lower personnel exposure to the hazardous materials [3].

Nuclear reactors operate at very high temperatures and strong irradiation environments that affect the materials properties. Determining how materials properties change with temperature and burnup is very important to understand the material performance during in-reactor operation or in case of accidents. Gd_2O_3 is mostly used in the form of a dilute solid solution in the UO_2 matrix and it is fabricated by the dry powder metallurgy route. During this process, Gd_2O_3 with wt. % fraction ranging from 2-10 % is firstly mixed with UO_2 using shaker mixer, then, the homogenized mix is pressed to 50 % theoretical density, and finally sintered at 1650°C for 3h in a hydrogen atmosphere using the conventional sintering methods [2].

A more effective reactivity control and a better fuel utilization can be achieved by the lumping the BA materials. Yahya et al. [4]have found that by lumping Gd_2O_3 in the center of the UO_2 fuel, a longer suppression of the excess of reactivity takes place and therefore a longer fuel cycle length can be achieved, mainly due to the higher self-shielding factor of the lumped BA design [4]. To understand the performance of the lumped BA fuel design, the thermo-physical properties of the bulk Gd_2O_3 as functions of the temperature and burn-up need to be determined. Most of the materials properties data is available for the UO_2-Gd_2O_3 solid solution and it is well documented in MATPRO series [5]. However, a very limited data is available for the bulk Gd_2O_3 properties such as crystal structure [6–8], thermal expansion coefficient [9,10], heat capacity [10,11], sinterability by spark plasma sintering (SPS) [12], and some mechanical properties [12–14].

The objective of this study is to summarize the available data of bulk Gd_2O_3 properties to identify the unavailable properties needed for the fuel performance analysis. This study also presents some of the newly measured properties of Gd_2O_3 including its sinterability, either by conventional sintering (CS) methods or microwave (MW) sintering as well as Gd_2O_3 thermal conductivity as a function of temperature. In addition, the densification tests after re-sintering were investigated to understand the irradiation-induced densification of Gd_2O_3.

2. Experimental procedures

For the sinterability study of Gd_2O_3 by CS and MW sintering methods, firstly, Gd_2O_3 powder was poured in a 13 mm-in-diameter steel mold and pressed using a uniaxial press under a load of 1000 kg (~ 74 MPa). After that, the pressed pellets were cold-isostatically pressed under a pressure of 500 MPa for 5 min to prepare green pellets. The green pellets were sintered using CS and MW sintering methods at temperatures up to 1600°C in an air environment. For CS, the heating rate was 10°C/min and the holding time was 2 h. For the MW sintering, the heating rate was 50°C/min and the samples were kept at the maximum temperatures for 20 minutes.

To understand the effect of irradiation on the Gd_2O_3 densification, re-sintering experiments were initially performed on the pre-sintered Gd_2O_3 with different initial densities. The initial density of the pre-sintered Gd_2O_3 varied by changing the initial sintering temperature up to 1500°C. The densification of the sintered Gd_2O_3 was measured using Archimedes principle according to ASTM B311 and its crystal structure was analyzed using X-ray diffractometry (XRD).

The thermal conductivities of the MW sintered Gd_2O_3 at different temperatures were determined from the measured thermal diffusivities, heat capacities, and thermal expansion coefficients at room temperature, 200°C, 400°C, 600°C, and 800°C. The thermal diffusivities were measured using the laser flash method and the differential scanning calorimetry was used to

measure the heat capacities of the sintered Gd_2O_3. The densities of the sintered samples at different temperatures were calculated using the thermal expansion coefficients with the measured density at room temperature.

3. Available properties of the bulk Gd_2O_3

3.1 Crystal structure and phase transformation

Gd_2O_3 crystallizes in cubic, monoclinic and hexagonal crystal structures. At room temperature, it crystalizes in the cubic crystal structure. As the temperature increases, Gd_2O_3 transforms to the monoclinic phase at a temperature of approximately 1,250°C, upon heating at temperatures about 2200°C or above, it transforms into the hexagonal phase [6,7]. The cubic to monoclinic phase transformation was found to be irreversible [6]. The lattice parameters of the three different crystal structures of Gd_2O_3 are shown in Table 1 [8].

Table 1. Gd_2O_3 crystal structures lattice parameters [8].

Crystal structure	Lattice parameters			
	a (nm)	b (nm)	c (nm)	β (°)
Cubic	1.0813 ±0.0005	-	-	-
Monoclinic	1.4061 ±0.0013	0.3566 ±0.0006	0.8760 ±0.0007	100.10 ±0.08
Hexagonal	0.376		5.89	

Since nuclear fuels are fabricated at temperatures above the cubic and monoclinic phase transformation and considering the lattice parameters of the cubic and monoclinic phase, a volume change of approximately 66 % would result during this phase transformation stage of Gd_2O_3. This volume change might contribute to the formation of interfacial gaps/cracks during the sintering process of the lumped Gd_2O_3 BA fuel design. Durazzo et al. [15] have investigated the effect of Gd_2O_3 phase transformation on the formation of interfacial cracks/gaps in UO_2-Gd_2O_3 solid solutions by sintering a cubic and monoclinic Gd_2O_3 with UO_2. The results of that study observed no change in the sintering behavior of UO_2-Gd_2O_3, this might be attributed to the cubic to monoclinic phase transformation occurrence at a temperature approximately close to the temperature at which the sintering of UO_2 starts (around 1200°C) [16]. Therefore, the volume change due to the phase transformation can be absorbed by the shrinkage due to sintering.

3.2 Thermal expansion coefficient

The thermal expansion coefficient (TEC) of Gd_2O_3 is an important factor that needs to be considered during the fabrication of the lumped BA fuel design and during reactor operation. Its importance comes from the possibility of the materials with a significantly different TEC to experience mechanical failure during the fabrication process.

Stecura et al. [9] have calculated the TEC of the cubic phase of Gd_2O_3 using X-ray diffractometry (Fig. 1). The samples were heated to a maximum temperature of 1150°C to avoid the phase transformation. As can be seen from Fig. 1, the TEC of the cubic Gd_2O_3 varies from about 6.8×10^{-6}/°C at room temperature to approximately 8.9×10^{-6}/°C at 1300°C.[9]

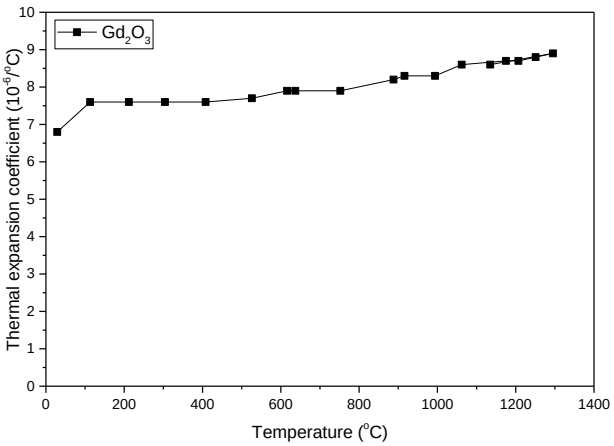

Fig.1. Thermal expansion coefficient of the cubic phase of Gd_2O_3.

The average TEC of the monoclinic Gd_2O_3 phase measured in the temperature range from 25-1000°C was 10.5×10^{-6}/°C [10]. The average TEC of UO_2 is around 12×10^{-6}/°C [2]. Therefore, interfacial cracks might form during the fabrication process of the lumped BA fuel design.

3.3 Heat capacity

The measured heat capacity of Gd_2O_3 sintered at 1300°C was found to be 0.342 kJ/g in the temperature range of 0-400°C, 0.526 kJ/g in the temperature range of 0-800°C, and 0.352 kJ/g in the temperature range of 0-1000°C respectively [10].

3.4 Mechanical properties

The elastic and shear moduli of the monoclinic phase of Gd_2O_3 as functions of temperature for samples with a relative density of 96.75 % was measured by Dole et al. [13] and the results are shown in Fig. 2 together with the fitting functions of the data.

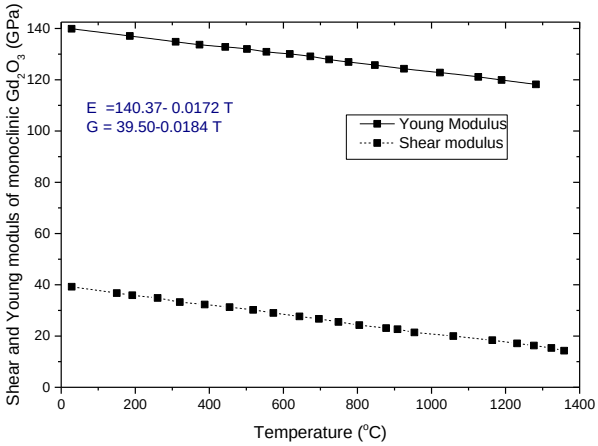

Fig. 2. Elastic and shear modulus of Gd_2O_3 as a function of temperature.[13]

Haglund et al. [14] measured the elastic properties of a polycrystalline monoclinic Gd_2O_3 with different initial porosity ranging from 2.5% to 36.7% and provided equations for the elastic properties as functions of the initial porosity using a 1st order linear curve fitting (Eqns. 1 and 2). The elastic properties were found to linearly decrease with the initial porosity of the sintered samples. The initial porosity of the sintered samples varied by changing the sintering temperature [14].

$$E = 150.26 (1- 1.76 P) \quad (1)$$
$$G = 58.85 (1-1.75 P) \quad (2)$$

Awin et al. [12] measured the elastic modulus of Gd_2O_3 after sintering at temperatures up to 1600°C. The elastic modulus of the samples sintered at 1600°C with a porosity of 0.45 % was about 160.71±9.60, which is close to the one predicted by Haglund et al. [14] considering the uncertainty of the experimental data.

3.5 Sintering behavior of Gd_2O_3

Studies about the sintering behavior of Gd_2O_3 with temperature are scarce. Only one study has recently been performed about the sintering behavior of Gd_2O_3 by SPS [12]. The relative density of Gd_2O_3 sintered at 1400, 1500, and 1600°C for 5 min under a pressure of 30 MPa in a vacuum atmosphere was 89.60, 97.63, and 99.65 % respectively [12]. The relative density of Gd_2O_3 sintered at 1850°C for 2h using the conventional sintering method was 96.75 % [13], which is lower than those obtained at 1500°C by SPS. This can be attributed to the higher heating rate and the different sintering mechanism of SPS.

4. Results and Discussion

4.1 Sintering behavior by CS and MW sintering

The relative densities of the conventionally sintered and MW sintered Gd_2O_3 as functions of the sintering temperature are shown in Fig. 3 together with those sintered by SPS [12].

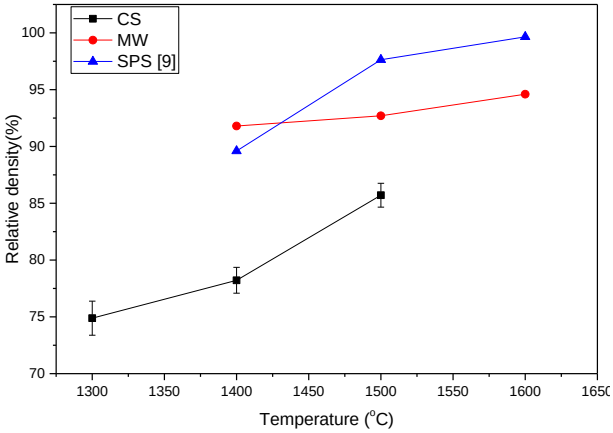

Fig. 3. Effect of sintering temperature on the relative density of Gd_2O_3 fabricated by C, MW or SPS.

As shown in Fig. 3, a much higher densification was observed in the samples sintered by MW and SPS at a lower temperature and with a shorter sintering time. This could be attributed to the different sintering mechanism in MW and SPS. In MW sintering, the heat is generated by the interaction between the powders and the electromagnetic waves developing a heat energy at every point of the materials [17]. In SPS, a low voltage and a continuous pulsed current are used to generate the heat. The heat, in turn, is transferred through the electrically conducting parts of the machine and through the conductive powder [18]. In SPS sintering (Fig.3), the densification was more enhanced when compared to MW sintering. This can be attributed to the particle rearrangement and agglomerates breakup facilitated by the applied pressure at high temperature and the higher heating rate [19].

4.2 Phase transformation

The XRD diffraction patterns of the CS Gd_2O_3 at different temperatures are shown in Fig. 4. The diffraction peaks of the cubic phase of Gd_2O_3 were observed when Gd_2O_3 was sintered at 1200°C. On the other hand, the diffraction peaks of the monoclinic phase of the Gd_2O_3 appeared in the samples sintered at 1300°C. This indicates that the cubic to monoclinic phase transformation occurs in a temperature range of 1200-1300°C, more specifically, at 1250°C as previously reported by the high-temperature XRD studies [6]. The monoclinic phase diffraction peaks were observed in the XRD diffraction patterns of the MW sintered Gd_2O_3 at temperatures between 1400-1600°C.

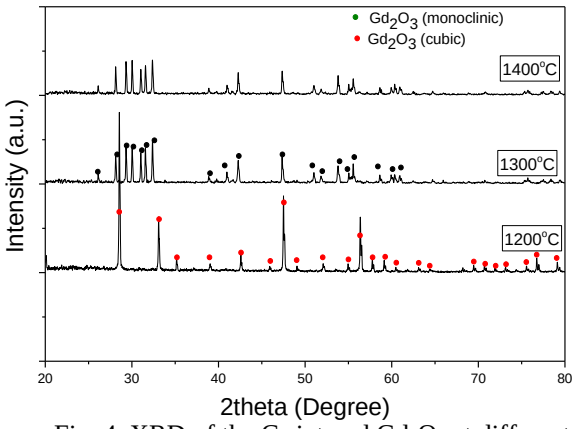

Fig. 4. XRD of the C sintered Gd_2O_3 at different temperatures.

4.3 Irradiation induced densification of Gd_2O_3

It was experimentally found that density increase during the out-of-reactor isothermal re-sintering tests is correlated with the in-reactor density changes [20]. Fig. 5 shows the effect of the re-sintering temperature on the relative density of Gd_2O_3 in order to show the amount of possible increase in the density of Gd_2O_3 during the in-reactor irradiation. As can be seen from Fig. 5, with increasing the re-sintering temperature, the relative density of Gd_2O_3 increases almost linearly. A higher relative density was achieved in the samples with a higher initial sintering temperature due to the decreased porosity. It can also be seen that all the samples were almost fully densified when the re-sintering temperature was 1600°C. This indicates that during the reactor operation, a full densification of Gd_2O_3 can be achieved.

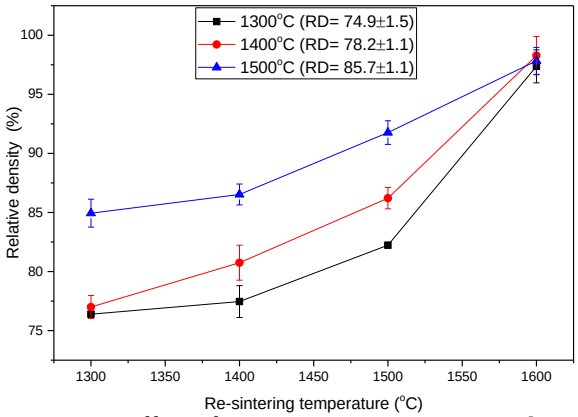

Fig. 5. Effect of re-sintering temperature on the relative density of Gd_2O_3.

4.4 Thermal conductivity

Fig. 5 shows the thermal conductivity of the 1500°C MW sintered Gd_2O_3 as a function of temperature. The data was corrected for the measured relative density using a modified Maxwell-Euken correlation given by Eq. 3 [21].

$$K_p = 1.0789\, K_{100}\left(\frac{1-P}{1+0.5P}\right) \quad (3)$$

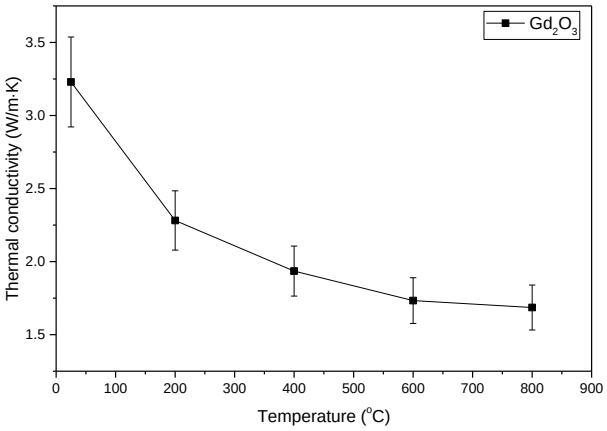

Fig. 6. The thermal conductivity of Gd_2O_3 with increasing the sintering temperature from 25°C to 800°C.

The thermal conductivity of Gd_2O_3 decreased with increasing the sintering temperature from 3.2 to 1.7 W/m·K. These values are much lower than the thermal conductivity of UO_2 [22].

5. Conclusions

The available properties of the bulk Gd_2O_3 were reviewed for the fuel performance analysis and it was found that since the cubic to monoclinic phase transformation of Gd_2O_3 is irreversible, the measurement of the TEC of the monoclinic phase of Gd_2O_3 as a function of temperature is needed. In addition, the dilatometric studies of the bulk Gd_2O_3 need to be performed in order to understand the sintering behavior of Gd_2O_3.

The densification of Gd_2O_3 with MW sintering and CS was investigated and it was compared with the previously reported densification results by SPS. It was found that a significant reduction in the sintering time and temperature can be achieved by the employment of MW and SPS due to the different sintering mechanism and the higher heating rate.

The irradiation-induced densification of Gd_2O_3 was investigated by the re-sintering tests. It was found that by the increasing the initial sintering temperature, the densification of Gd_2O_3 can be increased due to the decreased porosity with the initial sintering temperature.

The thermal conductivities of Gd_2O_3 as functions of temperature were measured by the laser flash method. The thermal conductivity of Gd_2O_3 decrease from approximately 3.2 W/m·K at room temperature to 1.7 W/m·K at 800°C. This lower thermal conductivity in comparison with the UO_2 thermal conductivity might

increase the fuel centerline temperature of the lumped BA design. Therefore, the temperature distribution in the lumped BA fuel design needs to be investigated in order to understand the possible effect of the lumped BA fuel design on the fuel performance.

Acknowledgments

This study was supported by the KUSTAR-KAIST institute at KAIST

REFERENCES

[1] B.M. Ma, Nuclear reactor materials and applications, Van Nostrand Reinhold Co, NEW YOK, 1983.

[2] Internaional Atomic Energy Agency, Characteristics and Use of urania-gadolinia fuels, 1995.

[3] L. Goldstein, A.A. Strasser, A comparison of gadolinia and boron for burnable poison applications in pressurized water reactors, Nucl. Technol. 60 (1983) 352–361. http://inis.iaea.org/Search/search.aspx?orig_q=RN:15036506.

[4] M.-S. Yahya, Y. Kim, Centrally-shielded burnable absorber for LWR fuel, in: Int. Congr. Adv. Nucl. Power Plants, American nuclear society, Fukui and Kyoto, 2017.

[5] L.J. Siefken, E.W. Coryell, E.A. Harvego, J.K. Hohorst, MATPRO-A Library of Materials Properties for Light-Water-Reactor Accident Analysis, 1998.

[6] R.S. Roth, S.J. Schneider, Phase equilibria in systems involving the rare-earth oxides. Part 1. Polymorphism of the oxides of the trivalent rare-earth ions, J. Res. Natl. Bur. Stand. Chem. 64 (1960) 309–316.

[7] F.X. Zhang, M. Lang, J.W. Wang, U. Becker, R.C. Ewing, Structural phase transitions of cubic Gd 2 O 3 at high pressures, Phys. Rev. B. 78 (2008) 64114. doi:10.1103/PhysRevB.78.064114.

[8] G. Adachi, N. Imanaka, The Binary Rare Earth Oxides, Chem. Rev. 98 (1998) 1479–1514. doi:10.1021/CR940055H.

[9] S. Stecura, W.J. Campbell, Thermal expansion and phase inversion of rare-earth oxides, 1960. doi:10.2172/4840970.

[10] C.E. CURTIS, J.R. JOHNSON, Ceramic Properties of Samarium Oxide and Gadolinium Oxide; X-Ray Studies of Other Rare-Earth Oxides and Some Compounds, J. Am. Ceram. Soc. 40 (1957) 15–19. doi:10.1111/j.1151-2916.1957.tb12541.x.

[11] B.H. Justice, E.F. Westrum, Thermophysical Properties of the Lanthanide Oxides. II. Heat Capacities, Thermodynamic Properties, and Some Energy Levels of Samarium(III), Gadolinium(III), and Ytterbium(III) Oxides From 10 To 350°K. 1, J. Phys. Chem. 67 (1963) 345–351. doi:10.1021/j100796a032.

[12] E.W. Awin, S. Sridar, R. Shabadi, R. Kumar, Structural, functional and mechanical properties of spark plasma sintered gadolinia (Gd2O3), Ceram. Int. 42 (2016) 1384–1391. doi:10.1016/j.ceramint.2015.09.080.

[13] S.L. Dole, J. Hunter, ELASTIC PROPERTIES OF SOME Gd2O3 HfO2 COMPOSITIONS, J. Nucl. Mater. 59 (1976) 207–214.

[14] J.A. HAGLUND, O. HUNTER, Elastic Properties of Polycrystalline Monoclinic Gd 2 O 3, J. Am. Ceram. Soc. 56 (1973) 327–330. doi:10.1111/j.1151-2916.1973.tb12506.x.

[15] M. Durazzo, R. Neto, A.M. Saliba-Silva, E.F. Urano De Carvalho, H.G. Riella, The role of Gd2O3 phase transition on UO2-Gd2O3 fuel sintering, Nucl. Technol. 182 (2013) 57–62. doi:10.1080/18811248.2007.9711574.

[16] M. Durazzo, A.M. Saliba-Silva, E.F. Urano De Carvalho, H.G. Riella, Sintering behavior of UO2-Gd2O3 fuel: Pore formation mechanism, J. Nucl. Mater. 433 (2013) 334–340. doi:10.1016/j.jnucmat.2012.09.033.

[17] A. Mondal, A. Upadhyaya, D. Agrawal, Microwave and Conventional Sintering of Premixed and Prealloyed Tungsten Heavy Alloys, (n.d.). https://www.researchgate.net/profile/Anupam_Mondal/publication/265924480_Microwave_and_Conventional_Sintering_of_Premixed_and_Prealloyed_Tungsten_Heavy_Alloys/links/56ea606b08ae25ede8313096.pdf (accessed August 18, 2017).

[18] O. Guillon, J. Gonzalez-Julian, B. Dargatz, T. Kessel, G. Schierning, J. Räthel, M. Herrmann, Field-assisted sintering technology/spark plasma sintering: Mechanisms, materials, and technology developments, Adv. Eng. Mater. 16 (2014) 830–849. doi:10.1002/adem.201300409.

[19] K. Rajeswari, U.S. Hareesh, R. Subasri, D. Chakravarty, R. Johnson, Comparative Evaluation of Spark Plasma (SPS), Microwave (MWS),Two stage sintering (TSS) and Conventional Sintering (CRH) on the densification and Micro structural Evolution of fully Stabilized Zirconia Ceramics, Sci. Sinter. 42 (2010) 259–267. doi:10.2298/SOS1003259R.

[20] M.D. Freshley, D.W. Brite, J.L. Daniel, P.E. Hart, Irradiation-induced densification of UO2 pellet fuel, J. Nucl. Mater. 62 (1976) 138–166. doi:10.1016/0022-3115(76)90013-1.

[21] P.G. Lucuta, H. Matzke, I.J. Hastings, A pragmatic approach to modelling thermal conductivity of irradiated UO2 fuel: Review and recommendations, J. Nucl. Mater. 232 (1996) 166–180. doi:10.1016/S0022-3115(96)00404-7.

[22] J. Fink, Thermophysical properties of uranium dioxide, J. Nucl. Mater. 279 (2000) 1–18. doi:10.1016/S0022-3115(99)00273-1.